Molecular Dynamics Simulations of Octyl Glucoside Micelles: Dynamic Properties

Stephen Bogusz, Richard M. Venable, and Richard W. Pastor*

Biophysics Laboratory, Center for Biologics Evaluation & Research, Food & Drug Administration, Rockville, Maryland 20852-1448

Received: December 13, 2000; In Final Form: April 20, 2001

Dynamic properties of octyl glucoside (OG) micelles were explored using molecular dynamics simulations. Systems studied included individual β-OG micelles containing 10, 20, 27, 34, 50, and 75 lipids; two 20 lipid β-OG micelles; a disperse solution of 27 β-OG; and four molecules of glucose. Calculated ^{13}C NMR T_1 relaxation times for the tail carbons of micelle aggregation numbers between 34 and 75 agreed well with experiment; these results are consistent with estimates of the micelle size based on translational diffusion. However, T_1's for the headgroup carbons, which couple strongly with the solvent, were too large. This was primarily due to the low viscosity of the TIP3P water model, and subsequent scaling of the relaxation times led to agreement with experiment for the carbons in the glucose ring, but not the exocyclic carbon; the likely reason for the latter discrepancy is a torsional potential barrier that is slightly too high. A detailed analysis of the micelle dynamics revealed shape changes on the time scale of tens to hundreds of picoseconds, while rotation and lipid diffusion within the micelle occur over nanoseconds. The primary components of NMR T_1 relaxation are lipid wobble and chain isomerization, as well as slower concerted motions on the time scale of the shape changes. Lipid lateral diffusion and overall micelle tumbling do not contribute significantly to NMR relaxation. Micelle self-assembly on the nanosecond time scale was also demonstrated. The two 20 lipid micelles merged and the 27 dispersed lipids aggregated, highlighting a new range of behavior accessible to molecular dynamics simulation.

I. Introduction

Micelles consist of molecules with a hydrophilic "head" and a hydrophobic "tail". They self-assemble above the "critical micelle concentration" (CMC). The structural and dynamic properties of micelles are important for the study of detergent properties and molecular self-assembly and development of drug delivery methods. In addition, micelles are used as surrogates for membranes because measurements of complexed peptides, proteins, or other organic molecules are often more tractable than with bilayers.

The nonionic detergent 1-*O*-*n*-octyl β-D-glucopyranoside, commonly referred to as octyl glucoside or OG, consists of an octane group attached to glucose, as diagramed in Figure 1. It forms micelles at a CMC of 20−25 mM.[1−9] OG has been widely used to solubilize and crystallize membrane proteins and to study membrane peptides.[10−18] α-OG (Figure 1) also forms micelles, though it has a lower solubility and CMC, and forms larger aggregates than β-OG.[6,19]

We have recently reported (paper I [20]) a simulation study of structural properties of OG micelles such as aggregate shape, tail length, dihedral angle distributions, hydrophobic surface area, headgroup cluster size, and location of water. These simulations included micelle sizes ranging from 10 to 75 surfactant molecules, thus covering much of the reported size range. The current work considers the dynamic properties determined from these simulations: micelle diffusion, rotation, shape change, and lipid diffusion and reorientation within the micelle. The time scales of these motions are calculated and related to ^{13}C NMR T_1 (spin lattice) relaxation times measured experimentally. Additionally, we present some preliminary results demonstrating micelle aggregation.

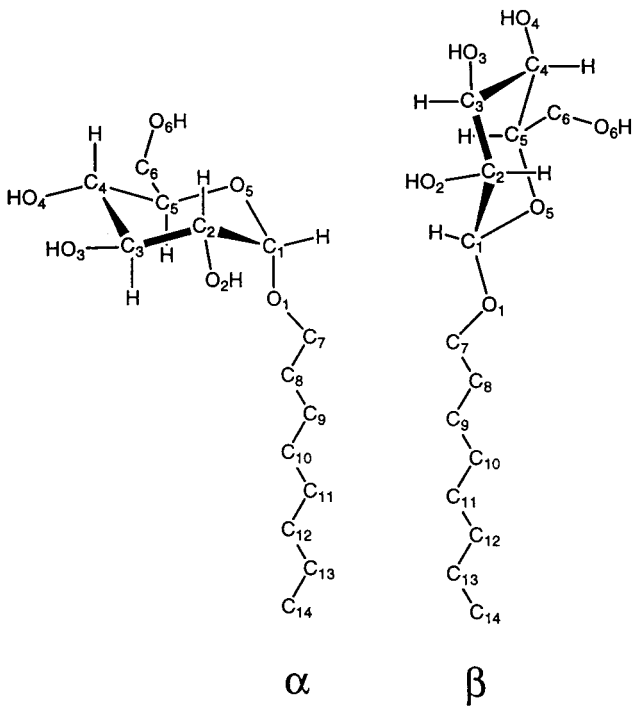

Figure 1. α-Octyl glucoside (left) and β-octyl glucoside (right) with heavy atom numbering scheme.

By way of outline, following a description of the methods of simulation, hydrodynamics and calculation of NMR relaxation times in section II, simulations of a glucose solution are presented in section III. An analysis of the rotational relaxation times and comparison with experimental T_1 values of glucose

10.1021/jp004475o
Published on Web 08/02/2001

confirmed the low viscosity of the water model and thereby justified the subsequent scaling of selected relaxation times for the micelle headgroup carbon atoms. Section IV considers the dynamics of the OG micelles, with particular emphasis on the interpretation of the NMR relaxation rates. The agreement of the simulation and experiment for the tails and supporting hydrodynamic estimates of the translational and rotational diffusion tensors of the entire micelle are used to develop a more detailed understanding of micelle dynamics. The disagreement between simulation and experiment for the heads is largely explained by deficiencies in the water model, as established in section III. The time scale of aggregation is explored in section V with simulations of two micelles and an OG solution. The results are further discussed in section VI.

II. Methods

Parameters and System Setup. Computations were carried out with the CHARMM (Chemistry at HARvard Molecular Mechanics)[21] simulation package version 26. Electrostatic interactions were evaluated with the Smooth Particle-Mesh Ewald (PME) method,[22] with a real space cutoff of 10 Å, a Gaussian width of 0.32 $Å^{-1}$, and a sixth order cubic spline for interpolation between grid points (described in detail in Feller et al.[23]). Grid sizes were between 1.0 and 1.5 Å/grid. A 2 fs time step was used, with covalent bonds to hydrogen atoms held rigid with the SHAKE algorithm.[24] The Lennard-Jones interactions were truncated between 8 and 10 Å with a smooth switching of the potential.

A series of 100 initial aggregate structures were each built for 10, 20, 27, 34, 50, and 75 β-OG (referred to as a 10mer, 20mer, etc.) and immersed in a previously equilibrated box of water molecules (details are reported in paper I). After energy minimization, the conformation with the most favorable water/lipid interaction energy was used as the initial condition for each of the MD simulations, except for those of the 10mer and 20mer where the conformation with the lowest tail accessible surface area was used.

Three new simulations are also reported. The first included 4 glucose and 712 water molecules in a 30 Å simulation cell (the concentration for which T_1 data are available), and will be referred to here as the "glucose simulation". The "two-micelle simulation" consisted of two 20 lipid micelle configurations chosen from the initial aggregate structures in a 60 Å cell. The micelles' centers of mass were placed along the box diagonal, 36 Å from one another. Initial conditions for the "solution simulation" were developed by placing 27 OG molecules randomly within a 45 Å cell. All lipids with overlap energies >10 kcal/mol were repositioned.

Simulation Technique. Simulations consisted of a heating phase, where the system temperature was increased from 98 to 298 K in 10 K increments over 20 ps, 100 ps of equilibration, 6 ns of production (where averages were accumulated) for the solution simulation, and 4 ns for the others. All simulations were carried out in the constant pressure and temperature (NPT) ensemble using the Langevin Piston method[25] with a piston mass of 250 amu and a collision frequency of 20 ps^{-1}. The temperature was maintained at 298 K by coupling to a Hoover thermostat[26] with a mass of 1000 kcal-ps^2.

Hydrodynamic Calculations. Estimates for micelle translational and rotational diffusion tensors were obtained using the bead model.[27−29] In general, a polymer can be modeled as a rigid set of N point sources of friction (or beads), and diffusion tensors are determined from the inverse of a $3N \times 3N$ hydrodynamic matrix containing the position and friction constant ζ of each bead. In the implementation adopted here, the heavy atoms comprising the micelle or glucose (including bound waters) interact via the Oseen tensor, and $\zeta = 4\pi\eta a$, where η is the solution viscosity and a is the hydrodynamic radius ($a = 1$ Å for heavy atoms of OG and 1.6 Å for oxygens of the required bound water).[27] For carbohydrates, a water was defined as bound if its interaction energy with the micelle was less than $-4k_BT$ (where k_B is Boltzmann's constant and T is the temperature); this cutoff value, which leads to about 1 water per hydroxyl group, was determined to be optimal for sucrose and a pentasaccharide.[30] The viscosity for the micelle solutions was set to 0.89 cP (the experimental value of water at 298 K) and to 1.02 cP for the glucose solution (the estimated value for a 5% solution at 303 K).[31] To take shape fluctuations of the micelle into account, diffusion tensors were determined using coordinate sets at 100 ps intervals (i.e., 40 coordinate sets for a 4 ns trajectory), and averages and standard errors were calculated. The translational and rotational diffusion constants, D_T and D_R, respectively, were evaluated as 1/3 of the trace of the corresponding tensor. The rotational anisotropy was defined as $D_{||}/D_{\perp}$, where $D_{\perp}$ is the average of the two closest eigenvalues of the diffusion tensor and $D_{||}$ is the remaining eigenvalue.

Calculation of NMR Relaxation Times. Assuming relaxation is due to dipolar interactions between the ^{13}C nucleus and its attached protons, the ^{13}C spin−lattice relaxation time, T_1, is given by[32]

$$\frac{1}{T_1} = \frac{N}{10}\left(\frac{\hbar\gamma_C\gamma_H}{r_{C-H}^3}\right)[J(\omega_H - \omega_C) + 3J(\omega_C) + 6J(\omega_H + \omega_C)] \quad (1)$$

where N is the number of hydrogens bound to the carbon, $\hbar$ is Plank's constant divided by 2π, r_{C-H} is the C−H bond length, γ_H, γ_C, ω_H, and ω_C are the gyromagnetic ratios and Larmor frequencies, respectively, of the ^{13}C and ^1H nuclei; $\omega_C = \gamma_C H$ and $\omega_H = \gamma_H H$, where H is the field strength. $C_2(t)$ is the second rank reorientational correlation function, and $J(\omega)$ its spectral density

$$C_2(t) = \langle P_2(\hat{\mu}(0)\cdot\hat{\mu}(t))\rangle \quad (2)$$

$$J(\omega) = \int_0^\infty C_2(t)\cos(\omega t)\, dt \quad (3)$$

where P_2 is the second-order Legendre polynomial and $\hat{\mu}(t)$ is the unit vector along the C−H bond direction at time t.

The reorientational correlation function for each C−H bond was calculated directly from the MD trajectory, averaged over all lipids (or glucose) for each carbon atom, and fit using nonlinear regression to a three exponential function:

$$C_2(t) = a_1 e^{-t/\tau_1} + a_2 e^{-t/\tau_2} + a_3 e^{-t/\tau_3} \quad (4)$$

where $a_1 + a_2 + a_3 = 1$ and τ_i are denoted decay times. Because no plateau value is included, the relaxation time, τ, is simply the integral of the correlation function; i.e.,

$$\tau = \sum a_i\tau_i \quad (5)$$

The spectral density of the correlation function defined by eq 4 is

$$J(\omega) = \frac{a_1\tau_1}{1 + (\omega\tau_1)^2} + \frac{a_2\tau_2}{1 + (\omega\tau_2)^2} + \frac{a_3\tau_3}{1 + (\omega\tau_3)^2} \quad (6)$$

TABLE 1: Reorientational Correlation Times τ (ps) and Spin Lattice Relaxation Rates $1/T_1$ (s^{-1}) for Glucose[a]

carbon	τ	$1/T_1$ (direct)	$1/T_1$ (scaled)	$1/T_1$ (expt)
1	15.8	0.32	0.74	0.690
2	15.6	0.32	0.73	0.690
3	15.5	0.32	0.73	0.725
4	15.6	0.32	0.73	0.725
5	15.8	0.32	0.74	0.699
6	16.4	0.67	1.53	1.388

[a] Scaled values include correction for temperature, solvent, and incorrect viscosity of water model. Experimental values from Benseni et al.[33]

When $\omega\tau_i \ll 1$ for each decay time, from eq 5, $J(\omega) = \tau$; this is the so-called motional narrowing regime. Inserting this value of $J(\omega)$ into eq 1 and assigning the constants leads to the simple expression for T_1:

$$\frac{1}{NT_1} = 2.0338 \times 10^{10}\tau \tag{7}$$

Fits of the correlation functions were limited to no more than three exponentials due to instabilities for more than five free parameters. To reduce statistical error, points were weighted by the inverse of their lipid-to-lipid variances, and fitting was cut off when $C(t)$ crossed zero.

III. Glucose Dynamics

Motions of the OG micelles such as overall rotation (or tumbling) and translation couple strongly with solvent, and are therefore dependent on the viscosity. Because the viscosity of the TIP3P water model is known to be low, approximately 0.35 cP,[23] it would be anticipated that the time scale of the preceding motions (and maybe others) would be significantly underestimated in the present simulations. To explore this effect, a simulation of a glucose solution was carried out and compared to experimental NMR T_1 values obtained at 250 MHz (hydrogen) and 303 K in D_2O,[33] and to hydrodynamic estimates of their rotational and translational diffusion coefficients.

As detailed in the preceding subsection, reorientational correlation functions were calculated for each CH bond, averaged over the four glucose, and fit to a three-exponential function. The functions contained a subpicosecond decay with very small amplitude (associated with rapid ring libration), and two longer decays (associated with tumbling for all carbons and, potentially, isomerization for C6). Because all three decay constants were small with respect to $1/\omega$, T_1 may be evaluated from eqs 5 and 7. Calculated τ and $1/T_1$ are listed for each carbon in Table 1 (note that $N = 1$ for the ring carbons, $N = 2$ for C6). The statistical errors in the relaxation times, $\sigma[\tau]$, are estimated at 5% using the approximate formula

$$\sigma[\tau] \approx \sqrt{\frac{2\tau}{N_s T_{run}}} \times 100\% \tag{8}$$

where N_s and T_{run} are the number of molecules and length of the simulation, respectively.

Equation 8 is based on the expression for the statistical error of a *point* of a correlation function derived by Zwanzig and Aliwadi[34] and has been shown to be a reasonable approximation for $\sigma[\tau]$ of a normalized correlation function.[35] The experimental values (final column of Table 1) of the spin−lattice relaxation rates are twice as high as the simulated values for all ring carbons. Because τ is dominated by tumbling for these carbons, one may surmise that the viscosity is too low by approximately a factor of 2.

A slightly more direct measure of rotational relaxation is obtained by evaluating $C_2(t)$ for the vector between carbons 1 and 4 of the glucose. From the simulation, $\tau_3 = 35.6$ ps. This decay time is approximately $1/6D_\perp$. From the hydrodynamic modeling, $1/6D_\perp = 74.6$ ps, or 2.10 times that obtained in the simulation.

Hence, we may conclude that the viscosity in the simulation is too low. Since overall rotation is frequency independent and linearly proportional to the viscosity, the relaxation associated with overall rotation must be linearly scaled. The scaling factor is the product of three terms: 0.90, the ratio of the viscosities of pure water at 303 and 298 K (the temperatures of the experiment and simulation, respectively); 1.23, the ratio of the viscosities of D_2O and H_2O at 298 K; and 2.1, the ratio of the hydrodynamic and simulated rotational correlation times noted in the preceding paragraph. The total scaling factor is $0.9 \times 1.23 \times 2.1 = 2.3$. The first two terms are standard in hydrodynamic treatments and would be necessary to apply even if the water model were accurate because conditions of the simulation and experiment were not identical. The third term is new and accounts for deficiencies in the TIP3P water model in arguably the simplest manner. As shown in the second to last column in Table 1, agreement with experiment is excellent after the total scaling factor is applied.

The results for carbon 6 bear further mention. Transitions of the C4−C5−C6−O6 dihedral angle could, in principle, affect the relaxation of C6. If rotation and isomerization are independent, and can be described with the relaxation times τ_R and τ_I, respectively, the relaxation time τ for a particular carbon can be written

$$\frac{1}{\tau} = \frac{1}{\tau_R} + \frac{1}{\tau_I} \tag{9}$$

When isomerizations are infrequent and rotation is fast, $\tau_I \gg \tau_R$ and, consequently, $\tau \approx \tau_R$. In the simulations, there was only a single isomerization for three of the glucose and none for the fourth. Hence, the relaxation of C6 is almost exclusively associated with rotation, and it is similar to the τ's of the ring carbons. As follows from eq 7 and is evident from Table 1, $1/T_1$ of C6 is approximately twice that of the ring carbons for both simulation and experiment. This result, however, does not imply that there are no transitions of the C4−C5−C6−O6 dihedral in a solution of glucose. Rather, only that rotation is sufficiently rapid so that the effect of transitions is not measured in the experiment.

IV. Micelle Dynamics

Following evaluations of reorientational correlation functions and T_1 relaxation times, motions are analyzed from slowest to fastest, and their potential contributions to the NMR decay are considered. Scaling of those motions that are strongly dependent upon viscosity resolves the initial disagreement with experiment for the ring carbons.

NMR Relaxation Times. The second rank correlation functions for each C−H bond were fit for each micelle to a three exponential function as already described. Only one exponential was required for C14 (see Figure 1 for numbering scheme), as the rapid rotation of the terminal methyl group overwhelms all other decay sources. Correlation functions for the glucose ring carbons (C1−C5) were almost superimposable and were averaged to reduce statistical error.

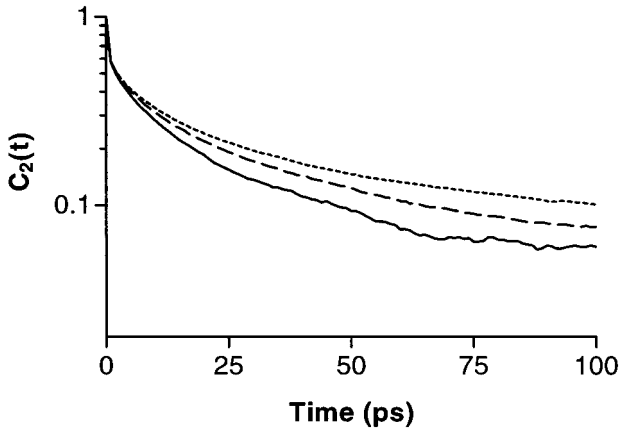

Figure 2. Reorientational correlation function (on a logarithmic scale) for C−H bond vectors of C12 for the 10mer (solid line), 34mer (dashed), and 75mer (dotted). Data averaged over all hydrogens and lipids.

TABLE 2: Parameters from a Three-Exponential Fit to the Reorientational Correlation Function for the Average of Carbons C1−C5 and for Carbons C8 and C13[a]

carbon	micelle	a_1	a_2	a_3	τ_1	τ_2	τ_3
<C1−C5>	10	0.132	0.573	0.295	1.31	25.5	177
	20	0.194	0.567	0.239	3.14	44.1	246
	27	0.220	0.634	0.146	4.19	57.4	404
	34	0.122	0.392	0.486	1.03	26.6	162
	50	0.161	0.378	0.461	2.18	44.1	256
	75	0.312	0.559	0.129	11.0	139	704
C8	10	0.377	0.431	0.192	0.951	24.1	176
	20	0.394	0.417	0.189	0.978	30.3	265
	27	0.434	0.415	0.151	1.34	43.3	312
	34	0.444	0.376	0.180	1.55	47.5	297
	50	0.421	0.386	0.193	1.28	46.8	393
	75	0.512	0.407	0.0807	2.89	103	1700
C13	10	0.531	0.403	0.0661	0.587	12.0	173
	20	0.560	0.368	0.0723	0.670	15.3	283
	27	0.547	0.376	0.0775	0.626	14.3	212
	34	0.567	0.369	0.0635	0.712	17.5	317
	50	0.557	0.360	0.0833	0.662	16.6	334
	75	0.625	0.321	0.0547	0.928	27.2	972

[a] Decay times in ps.

$C_2(t)$ of C12 for three different micelle sizes are plotted in Figure 2, and results of fitting for <C1−C5>, C8, and C13 are listed in Table 2. The two shorter decay times show only a weak increase with micelle size, while τ_3 shows a stronger dependence. The decay times are also influenced by position along the tail. Both τ_1 and τ_2 decrease monotonically for tail carbons as the C14 terminus is approached, as illustrated in Figure 3 for the 34mer. Values of τ_3, however, are comparable for all carbons (both head and tail). This implies that motions associated with τ_3 act uniformly on the whole lipid. These include lipid wobble and lateral diffusion, micelle shape fluctuations and rotation, all of which are expected to become slower as micelles become larger. The amplitude a_3 decreases from <C1−C5> to C13, indicating that the relative contributions of these motions to ^{13}C relaxation is greatest near the headgroup. Conversely, τ_1 and τ_2 include motions such as dihedral transitions that increase as the tail terminus is approached.[20] These motions are primarily modulated by the intramolecular potential[36] and thus are relatively unaffected by the micelle size.

Table 3 compares computed and experimental values of $1/T_1$ at two different magnetic strengths at temperatures close to that of the simulation.[37,38] As expected from the relaxation times in Table 2, the spin lattice relaxation rates are frequency dependent,

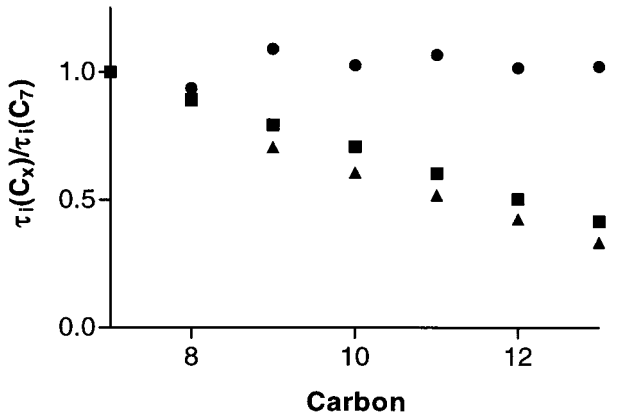

Figure 3. Decay constants τ_1 (squares), τ_2 (triangles), and τ_3 (circles) from three exponential fits of reorientational correlation functions for C−H bond vectors of tail carbons C7 to C13 for the 34mer. Values are divided by the corresponding value for C7 ($\tau_1 = 1.73$ ps, $\tau_2 = 53.3$ ps, and $\tau_3 = 316$ ps).

TABLE 3: Comparison of Calculated $1/T_1$ Values (in sec^{-1}) with Experimental Results of Soderman and Stilbs[38] ($\omega = 300$ MHz, $T = 300$ K, top) and Fischer[37] ($\omega = 270$ MHz, $T = 297$ K, bottom)[a]

carbon	10mer	20mer	27mer	34mer	50mer	75mer	expt
			300 MHz				
<1−5>	1.3	1.5	1.6	1.7	2.3	2.4	3.96
6	2.9	3.6	3.8	4.0	5.2	5.6	4.13
7	1.9	2.4	2.5	2.7	3.4	3.5	7.05
8	1.7	2.2	2.2	2.4	2.9	3.0	2.51
9	1.5	1.9	1.9	2.1	2.4	2.5	2.42
10	1.3	1.7	1.7	1.8	2.2	2.3	2.42
11	1.1	1.5	1.5	1.6	1.9	2.0	2.42
12	0.93	1.2	1.1	1.2	1.5	1.6	1.35
13	0.63	0.91	0.81	0.90	1.1	1.2	0.86
14	0.28	0.33	0.32	0.37	0.40	0.37	0.44
			270 MHz				
<1−5>	1.3	1.6	1.6	1.7	2.4	2.5	3.41
6	3.0	3.7	3.9	4.1	5.4	5.8	3.85
7	2.0	2.5	2.5	2.8	3.5	3.7	6.47
9	1.5	2.0	1.9	2.1	2.5	2.6	2.55
10	1.3	1.8	1.7	1.8	2.2	2.4	2.30
12	0.94	1.3	1.2	1.3	1.6	1.7	1.27

[a] Simulated results are only included when experimental data are available.

and eq 7 will not be accurate. From eq 8, the statistical error in the calculated T_1 values is approximately 10%, if it is assumed that the error is dominated by τ_3. The values for C8−C13 agree reasonably well with experiment for micelles in the 35−75 size range. In contrast, $1/T_1$ for the carbons in the glucose headgroup, <C1−C5>, and the linker carbon, C7, underestimate experiment by approximately a factor of 2; i.e., the reorientational relaxation in the simulation for these carbons is too rapid. These inconsistencies could be due to parameterization errors in either the glucose residue itself or in the sugar-octane linkage, or to the incorrect viscosity of the water model as already established for glucose.

Values for C6 agree with experiment, though the agreement is most likely fortuitous. The experimental values of $1/T_1$ for <C1−C5> and C6 are comparable, whereas they differ by approximately a factor of 2 for glucose (Table 1). As already discussed, the glucose results imply that ring rotation is significantly faster than isomerization of the C4−C5−C6−O6 dihedral angle. In contrast, the experimental micelle results imply that isomerization contributes to the relaxation of C6; i.e., ring rotation is sufficiently slowed to bring into the same

TABLE 4: Hydrodynamic Estimates of Translational Diffusion Constants (D_T) (in 10^{-6} cm^2 s^{-1}) and Reorientational Correlation Times (τ_R) at 298 K, 0.89 cP[a]

micelle	D_T	τ_R	τ_R (scaled)[b]
10	1.76 ± 0.01	2570 ± 40	1230
20	1.45 ± 0.01	4560 ± 50	2180
27	1.35 ± 0.003	5630 ± 60	2690
34	1.25 ± 0.003	7020 ± 60	3350
50	1.12 ± 0.002	9800 ± 80	4680
75	0.914 ± 0.01	14700 ± 90	7020

[a] All decay times in ps. [b] τ_R (scaled) is the expected correlation time when the solvent viscosity is too small by a factor of 2.1.

time scale as isomerization. For the micelle simulation, $1/T_1$ for C6 is approximately twice that of <C1−C5> at all calculated frequencies indicating that, as for glucose, the isomerization is not contributing significantly to the relaxation. These results suggest that the barrier for isomerization of C4−C5−C6−O6 is too high in the current parameter set.

Micelle Diffusion and Rotation. Estimates using the bead model (as described in section II) of the translational diffusion constant and rotational relaxation time $\tau_R = 1/6D_R$ for each micelle are listed in Table 4. The variation in these quantities for each micelle (which arises because of fluctuations in the micelle shape) is typically less than 1%. Because the rotational anisotropy was small, 1.1 to 1.3, the micelles can be reasonably approximated as spherical. In this case the preceding quantities can also be calculated from the Stokes−Einstein relationship with stick boundary conditions:[39,40]

$$D_T = \frac{k_B T}{6\pi\eta a} \qquad D_R = \frac{k_B T}{6\eta V} \tag{10}$$

where V is the volume and the other quantities have already been defined. Bound water molecules can be taken into account by increasing the unhydrated radius and volume.[27,39,41] Estimates of D_T and D_R using eq 10 with radii previously calculated from each micelle's radius of gyration (paper I, eq 5) with an additional 2 Å solvation shell are within 10% of the values listed in Table 4.

Dynamic light scattering experiments of OG micelles near the CMC and at 298 K yield $D_T = 0.94 \times 10^{-6}$ cm^2 sec^{-1} (ref 7) and 0.92×10^{-6} cm^2 sec^{-1} (ref 42). These values are consistent with a micelle size between 50 and 75 surfactants.

The preceding values imply that it is not realistic to directly evaluate the micelle translational diffusion constant from the present 4 ns simulations because of very high statistical errors. Specifically, the root-mean-squared displacement for an object with $D_T = 10^{-6}$ cm^2/s is approximately 15 Å, only about a single radius. Rather, estimates of D_T are best carried out with hydrodynamic methods.

Turning to rotation and NMR relaxation, the $C_2(t)$ will, in principle, contain a contribution from overall rotation if the angular anisotropy of the bond vector is not averaged out by faster motions. In analyzing the present simulations, however, this decay constant requires scaling because the viscosity of the water model is too low by a factor of 2.1. Dividing τ_R in Table 4 by 2.1 yields the relaxation times denoted τ_R(scaled) in the fourth column. The values τ_R(scaled) are 6 to 15 times larger than those of τ_3 for the CH vectors (Table 2). This result implies that "rigid body" rotational motion of the micelle does not make significant contribution to the ^{13}C T_1 relaxation. An additional correction for volume fraction increases the viscosity (increasing τ_R(scaled)) and thereby does not change the preceding conclusion.

Lipid Diffusion. Another potential source of C−H reorientation comes from the diffusion of individual lipids across the micelle surface. Figure 4 shows the dynamics of a single lipid in the 34mer on the 0.04, 0.4, and 4 ns time scales. The left-hand and middle images show fast motion including dihedral transitions and lipid "rattle", or oscillations in place. The right-hand image illustrates significant center of mass motion; i.e., the selected lipid has rotated approximately one-third of the micelle's circumference. It is not clear from this figure, however, whether the lipid is diffusing or the micelle is rotating. It is some of each, as demonstrated in the next two figures. Figure 5 highlights two lipids that are neighbors at the beginning of dynamics but are far apart after 4 ns. Hence, there is significant diffusion along the micelle surface. In Figure 6, lipids in two halves of the micelle at the start of the simulation are depicted in two different shades of gray. A rotation of approximately 90° is evident in the movement of the dark gray lipids from the right-hand side to the front of the micelle and the light gray lipids from the left-hand side to the rear. Additionally, there is some mixing of the light and dark gray lipids, indicating that lipid diffusion and micelle tumbling are on comparable time scales. If they are uncoupled, their contribution to NMR

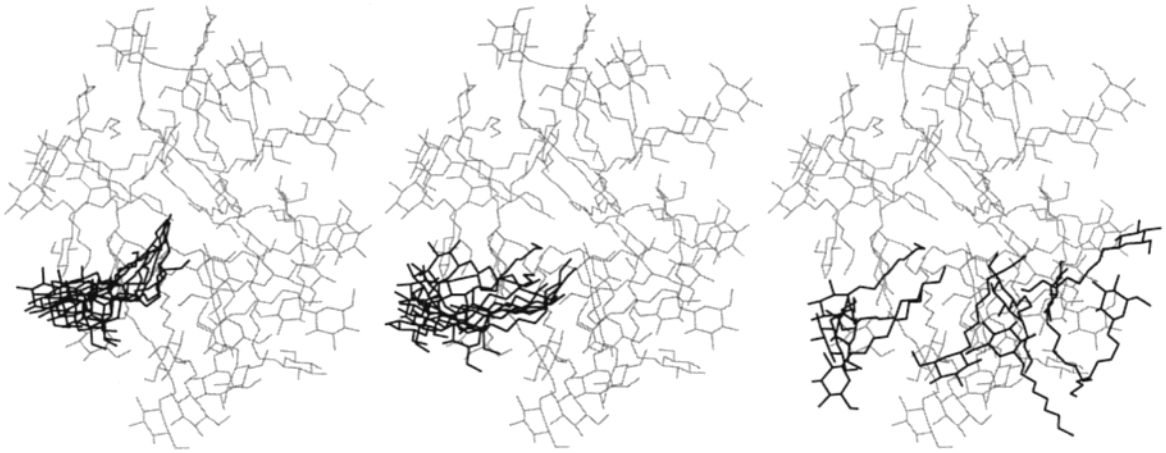

Figure 4. Trajectories of a single lipid from the 34mer simulation for 40 ps at 4 ps intervals (left), 400 ps at 40 ps intervals (center), and 4 ns at 400 ps intervals (right). Each trajectory starts at the beginning of the production run, and the center of mass motion of the micelle was removed from subsequent frames. Initial coordinates for the rest of the micelle are shown in gray to provide a sense of scale. The lipid was chosen for its mostly planar motion over the 4 ns; other lipids moved approximately the same distance but with more complex motion. In this and the remaining figures, water molecules are omitted for clarity.

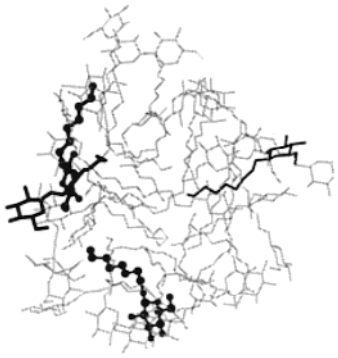

Figure 5. Initial and final coordinates of two lipids from the 34mer simulation. One lipid (shown as thick lines) is the same as in Figure 4. The other is a neighbor of the first in the initial coordinate frame, shown in ball-and-stick format. For both lipids, the thick lines are the initial coordinates and the medium-thick lines are the final coordinates. Final coordinates for the rest of the micelle are shown in thin lines to provide a sense of scale.

relaxation can be combined into a single decay time, τ_{RD}, with[43,44]

$$\frac{1}{\tau_{RD}} = \frac{1}{\tau_R} + \frac{1}{\tau_D} \tag{11}$$

where τ_R and τ_D are the decay constants for rotation and diffusion, respectively.

To estimate τ_{RD} and τ_D from simulation, $C_2(t)$ for the vector between the micelle center of mass and the O1 oxygen of each lipid was evaluated and averaged. This vector is relatively insensitive to fast lipid motions and shape fluctuations of the micelle, and its long time decay will be taken to be a surrogate of τ_{RD}. Columns two and three of Table 5 list values of τ_{RD} (obtained from single-exponential fits of $C_2(t)$ over 4 ns) and τ_D (from eq 11 and the values of τ_R(scaled)). Multiplying eq 11 by τ_{RD} and referring to Table 5 leads to the conclusions that lipid diffusion accounts for approximately 2/3 of τ_{RD} and micelle rotation accounts for 1/3. Note that the τ_{RD} are only about twice as large as τ_3 of the CH groups for the smaller micelles and the 75mer, and a factor of 5 larger for the 34 and 50mers. Such decays would be hard to isolate in 3-exponential fits if they were small in amplitude, and consequently would be averaged into the shorter decays. Hence, the combination of lipid diffusion and overall rotation could contribute to the T_1 relaxation.

Last, we comment on the relationship of τ_R and τ_D. If lipid lateral diffusion constants, D_L, were identical in each micelle, and if the micelles were perfectly spherical with radius a, τ_D would be expected to scale as a^2/D_L, and τ_R would scale as a^3. Inspection of Table 5 shows that this is not the case. Hence, the preceding assumptions are clearly too simple.

Micelle Shape Change. As already reported, micelle shapes differ significantly from spherical. The average eccentricity $\langle e \rangle \approx 0.6$ for aggregation numbers larger than 10, and the average of the ratios of the largest-to-smallest moments of inertia, $\langle I_3/I_1 \rangle$, varies between 1.3 and 1.7 for the different micelle sizes (paper I, Figure 6). Shape fluctuations are on the hundreds of picosecond time scale. This is illustrated in Figure 7, where the instantaneous ratios I_3/I_1 for the 34mer and 50mer are plotted are versus time. Some of the shape fluctuations are large and infrequent, such as the elongation of the 50mer to $I_3/I_1 = 2.2$ at 3.4 ns, indicating that a complete characterization of these events will require considerably longer simulations. While no micelle became completely spherical ($e = 0$), excursions to $e < 0.1$ took place on the 100 ps time scale.

To quantify the shape change rate, $C_2(t)$ of the principal moment of inertia was calculated for each micelle and fit to two exponentials over the range 0−500 ps; the two decay times are denoted τ_{S1} and τ_{S2}. The results of the fit are listed in Table

Figure 6. Micelle rotation and lipid diffusion for the 34mer. Lipids are colored according to their center of mass coordinates at the beginning of production dynamics: $x < 0$ in light gray and $x > 0$ in dark gray. Initial coordinates are shown at left, after 2 ns in center, final (4 ns) at right.

TABLE 5: Decay Times (in ps) of Assorted Micelle and Lipid Motions

micelle size	micelle rotation/ lipid translation			micelle shape change			lipid head reorientation			lipid tail reorientation		average relaxation parameters	
	τ_{RD}[a]	τ_D[b]	a_1[f]	τ_{S1}[c]	τ_{S2}[c]	a_1[f]	τ_{H1}[d]	τ_{H2}[d]	a_1[f]	τ_{T1}[e]	τ_{T2}[e]	$\langle\tau_1\rangle$[g]	$\langle\tau_3\rangle_{CH}$[h]
10	312	420	0.269	29.5	235	0.459	27.3	165	0.429	32.1	195	40	190
20	513	670	0.132	7.8	130	0.520	37.9	310	0.409	36.6	349	40	270
27	778	1100	0.421	14.9	221	0.465	37.1	281	0.385	36.1	327	47	330
34	1240	1970	0.470	48.2	504	0.335	28.1	249	0.625	79.6	516	46	250
50	1650	2550	0.125	71.1	1120	0.448	47.6	443	0.352	42.9	429	47	320
75	2780	4600	0.267	45.3	1550	0.787	140	2590	0.758	163	3130	57	1100

[a] τ_{RD} is the decay time from exponential fits of $C_2(t)$ for vectors from O1 to the center of the micelle. [b] Values of τ_D were obtained from eq 11, τ_{RD} and τ_R(scaled). [c] τ_{S1} and τ_{S2} are from two exponential fits of $C_2(t)$ for the principal eigenvector of the moment of inertia tensor and describe micelle shape change. [d] τ_{H1} and τ_{H2} are from two exponential fits of $C_2(t)$ for the vector between O1 and C4 and describe headgroup reorientation. [e] τ_{T1} and τ_{T2} are from two exponential fits of $C_2(t)$ for the vector between O1 and C14 and describe lipid tail reorientation. [f] For these two exponential fits, a_1 is the amplitude of the faster motion and $a_2 = 1 - a_1$. [g] $\langle\tau_1\rangle$ is the average of decay constants associated with isomerization of chain dihedral angles. [h] $\langle\tau_3\rangle_{CH}$ is the average of the longest fitted decay time for the CH vectors, neglecting the terminal methyl group.

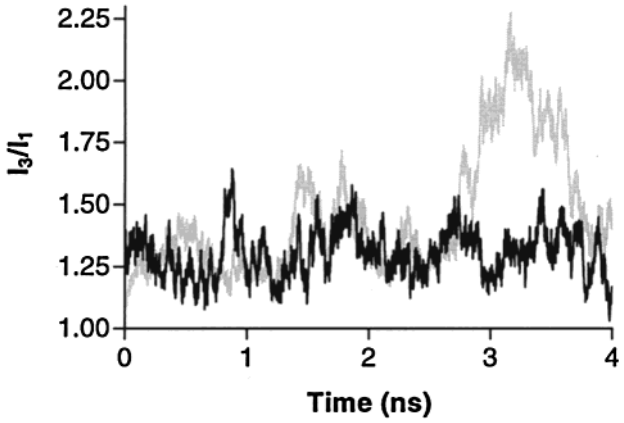

Figure 7. Ratio of largest to smallest components of the moments of inertia for the 34mer (black) and 50mer (light gray).

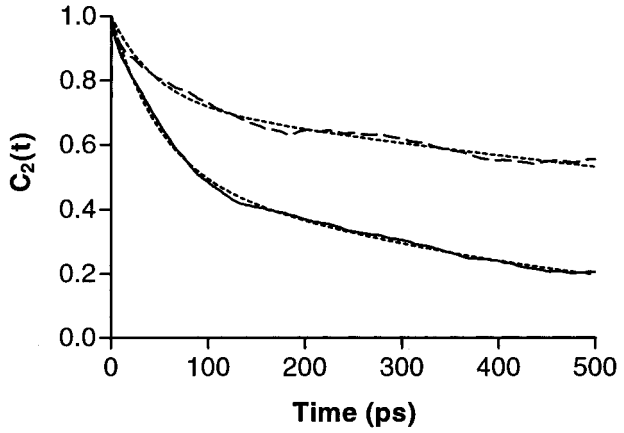

Figure 8. Reorientational correlation function of the principal moment of inertia for the 34mer (solid) and 75mer (dashed). Best fit of a 2 exponential function for each correlation function shown as a dotted lines.

5, and the correlation functions for the 34 and 50mers are shown in Figure 8. These decay constants are comparable to the two slower decay times of the CH vectors (Table 2).

Single Lipid Motions. The decay times just presented for shape change are clearly coupled with motions of single lipids, though not all of these motions will affect the orientation of CH vectors; e.g., translation of a lipid normal to the micelle surface changes micelle shape but does not rotate the molecule (see paper I, Figure 3 for an example). Correlation functions of two vectors, O1−C4 and O1−C14 were evaluated in order to determine the time scale of wobbling motions of the lipid heads and tails, respectively. These two vectors, rather than the molecular end-to-end vector, were chosen to discern possible "scissoring" or "swiveling" between the head and tail. The decay constants (with subscripts H and T for head and tail, respectively) and amplitudes from two exponential fits are listed in Table 5. The fast decays are likely associated with isomerizations of the chain dihedral angles. These were clearly evident, and tended to spread the chain out in a cone with respect to the headgroup; their relaxation time, τ_I, is given by[36]

$$\tau_I = (2k_{tg} + k_{gt})^{-1} \quad (12)$$

where k_{tg} and k_{gt} are the trans-to-gauche and gauche-to-trans rate constants, respectively. Values of τ_I were calculated from the rate constants described in paper I. They are relatively independent of micelle size, with an average of chain dihedrals ranging from 20 ps (C11−C12−C13−C14) to 54 ps (C7−C8−C9−C10) and 120 ps (O1−C7−C8−C9). These, as well as the average over all dihedrals $\langle\tau_I\rangle$ for each micelle (next to last column of Table 5), are, for the most part, similar to τ_{H1} and τ_{T1}. The averages of τ_3 of the CH vectors, denoted $\langle\tau_3\rangle_{CH}$, are listed in the final column of Table 5; these are comparable to τ_{H2} and τ_{T2}. Given the similarity of decay constants of the O1−C4 and O1−C14 vectors, it is likely that the head and tail are strongly coupled; i.e., that the slow reorientation of the lipid has a predominantly rigid body character, analogous, though not identical, to the "wobble" of lipids in bilayers.

Recalculation of NMR Relaxation Times for Ring Carbons. In the preceding subsections, motions were decomposed into micelle-rotation/lipid-diffusion (τ_{RD}), and fast (τ_{S1}) and slow (τ_{S2}) shape change, wobble of the lipid heads and tails (τ_{H2} and τ_{T2}), rapid reorientation of the heads and tails (τ_{H1} and τ_{T1}), and isomerizations ($\langle\tau_I\rangle$). All of these motions could, in principle, contribute to the relaxation of the CH vectors and, hence, to the NMR T_1 relaxation. As is clear from comparing Table 2 and Table 5, the contribution from micelle-rotation/lipid-diffusion is small. Lipid wobble, which is coupled to the slow shape change, is likely the major contribution to the slow decay of the CH vectors, while isomerization dominates the fast decay.

With these considerations in mind, it is difficult to propose a simple scaling to the viscosity as was successfully applied to glucose in section III; i.e., if the head and tail of each OG is tightly coupled, then the scaling should apply to both. However, from Table 3, only the ring carbons require significant scaling. Ignoring this consideration for purposes of a demonstration, a viscosity scaling factor of 2.47 appropriate to the experimental conditions (300 K, D_2O) can be calculated as the product of 0.956 (temperature dependence), 1.23 (D_2O), and 2.10 for (deficiencies in the water model). Applying this factor to τ_2 and τ_3 of the ring carbons yields $1/T_1$ values of 3.2 s^{-1}, 3.9 s^{-1}, and 4.0 s^{-1} for the 34mer, 50mer, and 75mer, respectively. The latter two values compare favorably with the experimental value of 3.96 s^{-1}.

V. Time Scale of Micelle Formation

To explore the dynamics of micelle aggregation, two 20-lipid micelles were placed together within a 60 Å cell and allowed to diffuse freely. As shown in Figure 9, the micelles come into contact within 300 ps and fully join by 3 ns. During this process the accessible surface area (ASA) of the hydrophobic tails drops from 58 ± 1 to 25 ± 2 $Å^2$ per tail, as averaged over the first and last 100 ps, respectively. (Values were calculated using the Lee and Richards method[45] with a probe radius of 1.6 Å.) The final ASA value for the 40-lipid micelle is between that of the 34mer and 50mer (33.3 ± 0.2 $Å^2$ and 23.1 ± 0.1 $Å^2$, respectively) as reported in paper I. This decrease in the exposed hydrophobic surface area is likely the main driving force behind the merger.

Even more impressive is the aggregation of an OG micelle from a solution of 27 randomly placed lipids, as illustrated in Figure 10. The lipids form a number of small clusters that rapidly merge into two micelles, which then join together to form a single micelle. The ASA of the tails decreases from 252 ± 2 $Å^2$ to 57 ± 2 $Å^2$ (again averaged over the first 100 and last 100 ps) per tail during 6 ns of simulation. The final ASA of the merged solution is higher than the average ASA of the 27mer simulation, 38.8 ± 0.2 $Å^2$ (paper I), suggesting that this micelle is not completely equilibrated.

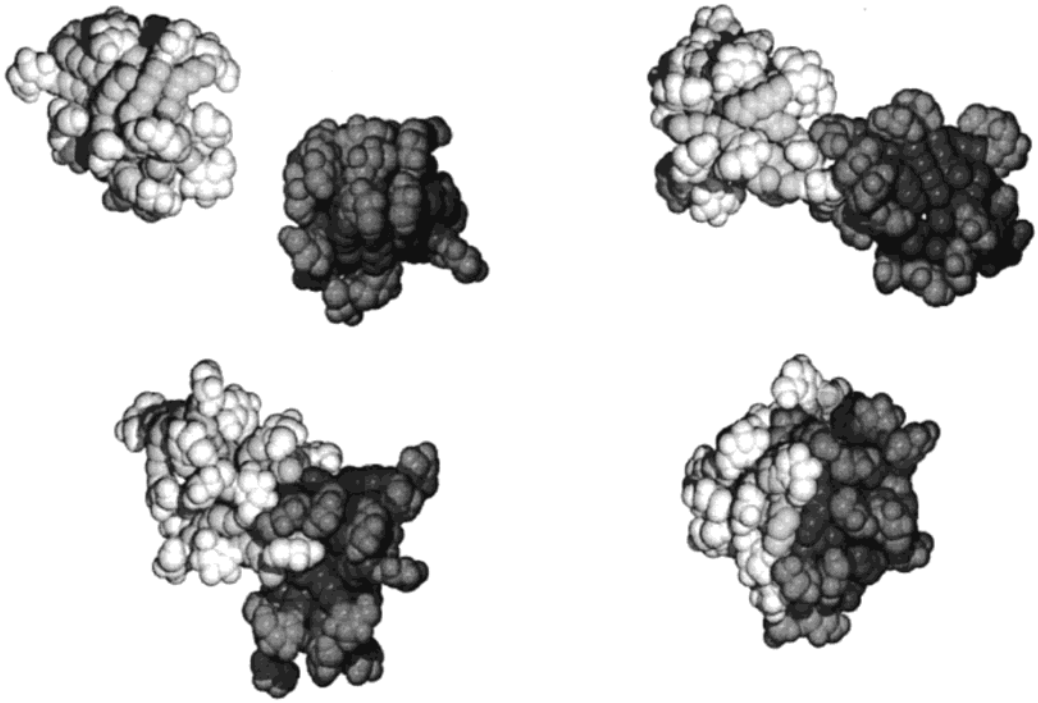

Figure 9. Merger of two 20-lipid micelles after 0.1 ns (top left), 1.0 ns (top right), 2.5 ns (bottom left), and 6.0 ns (bottom right) of production dynamics. One micelle is in light gray, the other in dark gray. Tail carbons are colored a slightly darker shade than head carbons.

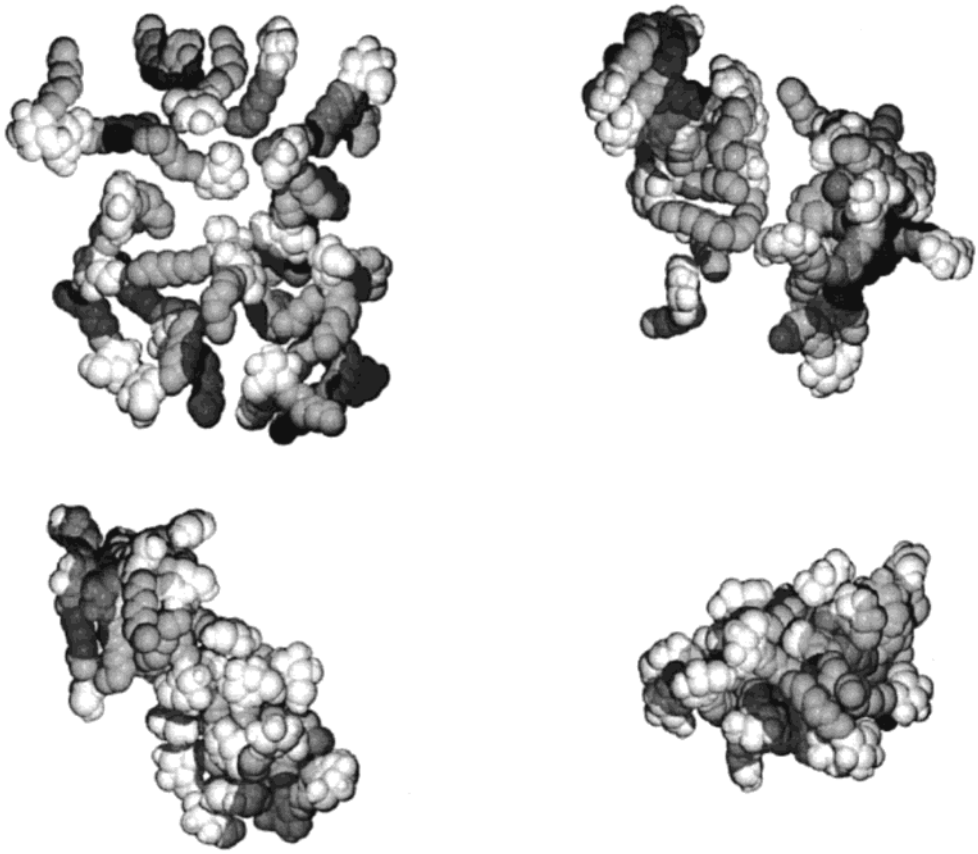

Figure 10. Aggregation of 27-lipid OG solution. Initial conditions (top left), after 0.4 ns (top right), 2.0 ns (bottom left), and 4.0 ns (bottom right) of production dynamics. Tail carbons are colored a slightly darker shade than head carbons.

VI. Discussion

The results of this study bear on both simulation methodology and micelles. We begin with the methodological issues.

A comparison of simulated and experimental NMR T_1 relaxation times for solutions of glucose and of octylglucoside micelles uncovered several errors in the potential energy parameters used in the simulation. First, and in accord with our previous findings for pure TIP3P water,[23] is that the viscosities of the glucose and micelle solutions underestimated experiment by approximately a factor of 2. This result was deduced for the

glucose solution by considering the ring carbons, where the T_1's are primarily determined by molecular rotation and the molecular vector between carbons 1 and 4. Because rotational diffusion constants are simple to calculate by hydrodynamic methods, it was straightforward to determine the scaling factor between the simulated and experimental solutions, scale the reorientational correlation time of the CH vectors by this factor, and thereby obtain agreement with experiment. The micelles were more difficult to analyze, because many motions contribute to the T_1. Nevertheless, the same scaling procedure applied for glucose led to agreement of experiment and simulation for the ring carbons of the 75mer. While it is noteworthy that evaluation of a dynamic quantity provided a test of the parameters (force field development is typically carried out using equilibrium properties), the incorrect viscosity of the TIP3P model undermines its usefulness for MD. A second parameter error involves the C4−C5−C6−O6 dihedral angle of glucose. This angle is relatively inflexible in the simulation, while the T_1 data imply that it isomerizes on the several hundred ps time scale. Reparametrization of this angle and possibly the dihedral angle that links glucose and octane in octyl glucoside is required. In contrast, good agreement with NMR experiments was obtained for the tails (Table 3), suggesting that the parametrization of acyl chains is acceptable. This is in accord with most results from simulations of lipid bilayers, where the equilibrium and dynamics of the chains agree well with experiment.[46]

The present results bear similarities and differences to those obtained in simulations by Tieleman et al.[47] of a dodecylphosphocholine (DPC) micelle using the GROMOS potential energy function with the SPC water model.[48] The calculated $1/T_1$ values for the tails agreed with experiment, again indicating the general robustness of hydrocarbon parameters. However, the headgroups were half the experimental values, instead of twice experiment as obtained here for OG micelles. Significant differences of the two simulations include water model, time step, bond constraints, and lipid potential energy functions, all of which may alter the solution viscosity and surface interactions, thereby account for the relative difference in the headgroup dynamics.

Turning to the behavior of micelles, the present simulations show a wide range motions, from rapid isomerization of the tail dihedral angles, angular reorientation (or wobble) of the lipids, shape changes of the micelle, lateral diffusion of the lipids, to rotation and translation of the entire micelle. These motions, however, are not all separable. For example, micelle shape changes (as determined by fluctuations in the moment of inertia) are on the same time scale as lipid isomerization and wobble (Table 5). It is reasonable to surmise that they are partially coupled; i.e., compression of the micelle from spherical to oblate will rotate some of the lipids, and isomerization of a lipid tail could effect a small shape change in the micelle. Some of the fast shape changes observed in previous simulations of sodium octanoate micelles[49−52] are likely associated with chain isomerizations. As noted in paper I, isomerization rates in micelles and bilayers of OG are comparable (paper I, Table 4), so isomerization arguably drives the fast shape changes of the micelle, rather than vice versa. In contrast, the tail angles with respect to the micelle centers and bilayer normal are not equal (paper I, Table 3); i.e., the degree of wobble is sensitive to the shape and surface roughness of the micelle. In this case, the slow shape fluctuations of the micelle would partially drive the lipid long axis reorientation.

The present simulations highlight the complexity of micelle rotation. As is clear from Figures 4−6 and Tables 4 and 5, individual lipids laterally diffuse somewhat faster than the micelle rotates. Additionally, the micelle undergoes substantial shape changes on the several hundred ps time scale (Figure 7, and paper I, Figure 3). A rigid sphere model (eq 10) should only be used for a general estimate of rotational time scales and may not be appropriate for analyzing a particular experiment. In contrast, the rigid sphere model provides a good estimate of the translational diffusion constant, as long as hydration is taken into account. This is because translational diffusion is much less sensitive to deviations from sphericity than is rotational diffusion.

Some of these results are expected to be micelle dependent. Simulations of lysophosphatidylethanolamine[53] and sodium dodecyl sulfate (SDS)[54] micelles did not show significant shape changes or lipid diffusion. In contrast, lipid diffusion was 10-fold faster than micelle rotation in simulations of sodium octanoate micelles,[49] and large lipid fluctuations were observed in simulations of an SDS micelle.[55] Given that some of the fluctuations observed here are on the ns time scale, it is reasonable to extend earlier simulations that were restricted to 100 ps by limitations of computer time.

The complexity of motions observed in the simulation implies that simple models will be insufficient when interpreting many experiments. This was stressed more than a decade ago by Watanabe and Klein[51] who observed substantial shape fluctuations in their simulations of a sodium octanoate micelle, while earlier analysis of small angle neutron scattering (SANS) data had neglected this effect. Similar considerations hold for interpreting NMR results. For the present systems, the relative importance of shape fluctuations in averaging out the anisotropy of the CH vectors implies that lateral lipid diffusion and micelle rotation play a relatively minor role in the ^{13}C T_1 relaxation. Hence, approaches based on a rigid sphere[32] or symmetric top,[56] so useful for analyzing protein dynamics, are not appropriate for OG micelles and should only be applied with caution to others.

Finally, the demonstrations of micelle aggregation (Figures 9 and 10) and micelle disassociation (paper I, Figure 2) add to a growing body of studies where large scale rearrangements of surfactants have been successfully simulated with atom-level models.[57−59] Several cautions, however, must be noted. Clearly, a quantitative analysis of simulated aggregation must await an accurate water model; i.e., the time scales in the present simulation are probably in error by approximately a factor of 2. Concentration effects are also a concern, as discussed in paper I. The nominal concentration of the simulated OG solution is 490 mM, twenty times that of the CMC. At such a high concentration one would expect the formation of extremely large micelles. However, given that it is impossible for the system to assemble into spherical micelles larger than the total number of surfactants in the unit cell, the effective concentration is much smaller than 490 mM. Carrying out the simulation at the CMC would not be trivial: the system would need to be twenty times larger, and the condensation would likely take considerably more time.

Despite the difficulties noted above, the time scales now possible for MD simulations provide opportunity to study micelle formation and the components of lipid movement that contribute to NMR measurements. Future increases in computational speed will allow an even greater understanding of the longtime behavior of these and similar systems.

Acknowledgment. We thank Bernard Brooks of the National Heart, Lung, and Blood Institute at the National Institutes of Health for the use of LoBoS, a Beowulf class supercomputer.

Computations also utilized the IBM SP supercomputer at the Center for Information Technology, NIH, Bethesda, MD.

References and Notes

(1) Shinoda, K.; Yamanaka, T.; Kinoshita, K. *J. Phys. Chem.* **1959**, *63*, 648−650.
(2) Shinoda, K.; Yamaguchi, T.; Hori, R. *Bull. Chem. Soc. Jpn.* **1961**, *34*, 237−241.
(3) Mukerjee, P.; Perrin, J.; Witzke, E. *J. Pharm. Sci.* **1970**, *59*, 1513−5.
(4) De Grip, W. J.; Bovee-Geurts, P. H. M. *Chem. Phys. Lipids* **1979**, *23*, 321−335.
(5) Lee, K. H.; De Mayo, P. *Photochem. Photobiol.* **1980**, *31*, 311−314.
(6) Straathof, A. J. J.; van Bekkum, H.; Kieboom, A. P. G. *Starch/Starke* **1988**, *40*, 438−440.
(7) Focher, B.; Savelli, G.; Torri, G.; Vecchio, G.; McKenzie, D. C.; Nicoli, D. F.; Bunton, C. A. *Chem. Phys. Lett.* **1989**, *158*, 491−494.
(8) Lorber, B.; Bishop, J. B.; DeLucas, L. J. *Biochim. Biophys. Acta* **1990**, *1023*, 254−65.
(9) Aoudia, M.; Zana, R. *J. Colloid Interface Sci.* **1998**, *206*, 158−167.
(10) Laczko-Hollosi, I.; Hollosi, M.; Lee, V. M.; Mantsch, H. H. *Eur. Biophys. J.* **1992**, *21*, 345−8.
(11) Laczko-Hollosi, I.; Hollosi, M.; Lee, V. M. Y.; Mantsch, H. H. *Peptides* **1992**, 527−528.
(12) Hollosi, M.; Ismail, A. A.; Mantsch, H. H.; Penke, B.; Varadi, I. G.; Toth, G. K.; Laczko, I.; Kurucz, I.; Nagy, Z.; Fasman, G. D.; Rajnavolgyi, E. *Eur. J. Biochem.* **1992**, *206*, 421−425.
(13) Otvos, L.; Szendrei, G. I.; Lee, V. M. Y.; Mantsch, H. H. *FEBS* **1993**, *211*, 249−257.
(14) Hantgan, R. R.; Braaten, J. V.; Rocco, M. *Biochemistry* **1993**, *32*, 3935−3941.
(15) Seigneuret, M.; Levy, D. *J. Biomol. NMR* **1995**, *5*, 345−352.
(16) D'Aprano, A.; Lamesa, C.; Proietti, N.; Sesta, B.; Tatone, S. *J. Solution Chem.* **1994**, *23*, 1331−1346.
(17) Kano, K.; Ishimura, T. *J. Chem. Soc., Perkin Trans.* **1995**, *2*, 1655−1660.
(18) Le Guerneve, C.; Seigneuret, M. *J. Biochem. NMR* **1996**, *8*, 219−222.
(19) Nilsson, F.; Soderman, O.; Johansson, I. *Langmuir* **1996**, *12*, 902−908.
(20) Bogusz, S.; Venable, R. M.; Pastor, R. W. *J. Phys. Chem. B* **2000**, *104*, 5462−5470.
(21) Brooks, B. R.; Bruccoleri, R. E.; Olafson, B. D.; States, D., J.; Swaminathan, S.; Karplus, M. *J. Comput. Chem.* **1983**, *4*, 187−217.
(22) Essmann, U.; Perera, L.; Berkowitz, M. L.; Darden, T.; Lee, H.; Pedersen, L. G. *J. Chem. Phys.* **1995**, *103*, 8577−8593.
(23) Feller, S. E.; Pastor, R. W.; Rojnuckarin, A.; Bogusz, S.; Brooks, B. R. *J. Phys. Chem.* **1996**, *100*, 17011−17020.
(24) Ryckaert, J. P.; Ciccotti, G.; Berendsen, H. J. C. *J. Comput. Phys.* **1977**, *23*, 327−341.
(25) Feller, S. E.; Zhang, Y.; Pastor, R. W.; Brooks, B. R. *J. Chem. Phys.* **1995**, *103*, 4613−4621.
(26) Hoover, W. G. *Phys. Rev. A* **1985**, *31*, 1695.
(27) Venable, R. M.; Pastor, R. W. *Biopolymers* **1988**, *27*, 1001−14.
(28) Wegener, W. *Biopolymers* **1981**, *20*, 303−326.
(29) Garcia de la Torre, J.; Bloomfield, V. A. *Q. Rev. Biophys.* **1981**, *14*, 85−138.
(30) Rundlof, T.; Venable, R. M.; Pastor, R. W.; Kowalewski, J.; Widmalm, G. *J. Am. Chem. Soc.* **1999**, *121*, 11847−11854.
(31) Weast, R. C. *CRC Handbook of Chemistry and Physics*, 62nd ed.; CRC Press: Boca Raton, Florida, 1982.
(32) Lipari, G.; Szabo, A. *J. Am. Chem. Soc.* **1982**, *104*, 4546−4559.
(33) Benesi, A. J.; Brant, D. A. *Macromolecules* **1985**, *18*, 1109−1116.
(34) Zwanzig, R.; Ailawadi, N. K. *Phys. Rev.* **1969**, *182*, 280−283.
(35) Pastor, R. W. In *The Molecular Dynamics of Liquid Crystals*; Luckhurst, G. R., Veracini, C. A., Eds.; Kluwer Academic Publishers: The Netherlands, 1994; pp 85−138.
(36) Zhang, Y.; Venable, R. M.; Pastor, R. W. *J. Phys. Chem.* **1996**, *100*, 2652−2660.
(37) Fischer, T. H. *Mol. Cryst. Liq. Cryst.* **1983**, *92*, 7−13.
(38) Soderman, O.; Stilbs, P. *Chem. Phys. Lipids* **1986**, *41*, 117−122.
(39) Cantor, C. R.; Schimmel, P. R. *Biophysical Chemistry, PartII: Techniques for the Study of Biological Structure and Function*; W. H. Freeman and Co.: San Francisco, 1980.
(40) Einstein, A. *Investigations on the Theory of Brownian Movement*; Dover: New York, 1956.
(41) Teller, D. C.; Swanson, E.; de Haen, C. *Methods Enzymol.* **1979**, *61*, 103.
(42) D'Aprano, A.; Giordano, R.; Jannelli, M. P.; Magazu, S.; Maisano, G.; Sesta, B. *J. Mol. Struct.* **1996**, *383*, 177−182.
(43) Wennerstrom, H.; Lindman, B.; Soderman, O.; Drakenberg, T.; Rosenholm, J. B. *J. Am. Chem. Soc.* **1979**, *101*, 6860−6864.
(44) Nery, H.; Soderman, O.; Carnet, D.; Walderhaug, H.; Lindman, B. *J. Phys. Chem.* **1986**, *90*, 5802−5808.
(45) Lee, B.; Richards, F. M. *J. Mol. Biol.* **1971**, *55*, 379.
(46) Forrest, L. R.; Sansom, M. S. P. *Curr. Op. Struct. Biol.* **2000**, *10*, 174−181.
(47) Tieleman, D. P.; van der Spoel, D.; Berendsen, H. J. C. *J. Phys. Chem. B* **2000**, *104*, 6380−6388.
(48) Berendsen, H. J. C.; Postma, J. P. M.; van Gunsteren, W. F.; Hermans, J. In *Intermolecular Forces: Proceedings of the 14th Jerusalem Symposium on Quantum Chemistry and Biochemistry*; Pullman, B., Ed.; Reidel: Dordrecht, Holland, 1981; pp 331−342.
(49) Jonsson, B.; Edholm, O.; Teleman, O. *J. Chem. Phys.* **1986**, *85*, 2259−2271.
(50) Shelley, J.; Watanabe, K.; Klein, M. L. *Electrochim. Acta* **1991**, *36*, 1729−1734.
(51) Watanabe, K.; Klein, M. *J. Phys. Chem.* **1989**, *93*, 6897−6901.
(52) Shelley, J. C.; Sprik, M.; Klein, M. L. *Langmuir* **1993**, *9*, 916−926.
(53) Wendoloski, J. J.; Kimatian, S. J.; Schutt, C. E.; Salemme, F. R. *Science* **1989**, *243*, 636−638.
(54) Shelley, J.; Watanabe, K.; Klein, M. L. *Int. J. Quantum Chem.* **1990**, 103−117.
(55) Mackerell, A. D. *J. Phys. Chem.* **1995**, *99*, 1846−1855.
(56) Tjandra, N.; Feller, S. E.; Pastor, R. W.; Bax, A. *J. Am. Chem. Soc.* **1995**, *117*, 12562−12566.
(57) Salaniwal, S.; Cui, S. T.; Cummings, P. T.; Cochran, H. D. *Langmuir* **1999**, *15*, 5188−5192.
(58) Maillet, J. B.; Lachet, V.; Coveney, P. V. *Phys. Chem. Chem. Phys.* **1999**, *1*, 5227−5290.
(59) Marrink, S. J.; Tieleman, D. P.; Mark, A. E. *J. Phys. Chem. B* **2000**, *104*, 12165−12173.